A METHOD BASED ON EJECTOR TECHNOLOGY TO SUPPRESS THE INFRARED RADIATION OF THE SPECIAL VEHICLE EXHAUST GAS

by

Yunsong FENG [a,b,c*], ***Wei JIN*** [a,b,c], ***Jin WANG*** [a,b,c], ***and Yuan LU*** [a,b,c]

[a] Infrared and Low Temperature Plasma Key Laboratory of Anhui Province, NUDT, Hefei, China
[b] Advanced Laser Technology Laboratory of Anhui Province, NUDT, Hefei, China
[c] State Key Laboratory of Pulsed Power Laser Technology, NUDT, Hefei, China

Original scientific paper
https://doi.org/10.2298/TSCI200611315F

In this study, a method based on ejector technology is proposed to effectively suppress the infrared radiation associated with the exhaust gas of special vehicles such as tanks, armored vehicles, and missile carriers. These vehicles emit exhaust gases at very high temperatures. First, a mathematical model of the exhaust pipe was established for the exhaust system of a certain type of special vehicle. Then, the 3-D flow field outside the exhaust pipe was numerically simulated using FLUENT 6.3 software. Thus, the temperature, pressure, and density of the exhaust-gas-flow field before and after adopting the proposed ejector technique were obtained. Second, the statistical narrowband model based on the Lorentzian profile was used to determine the average absorption coefficient of a narrow band. Then, the finite volume method was used to solve the radiation transfer equation in the gaseous medium. Finally, the spectral radiation brightness and mid-infrared radiation intensity distribution of the exhaust gas before and after adopting the ejector technique were obtained. Results show that the proposed method considerably decreased the infrared radiation intensity of the exhaust gas by approximately 70%. Thus, using the proposed ejector technology, the infrared radiation associated with the exhaust system of special vehicles can be effectively suppressed.

Key words: *ejector technique, special vehicle, exhaust gas, flow field, temperature, infrared radiation, finite volume method*

Introduction

Generally, special vehicles, such as tanks, armored vehicles, and missile carriers, require high power Diesel engines for propulsion. During the driving process, the temperature in the exhaust pipe can become as high as 800 °C and that of the exhaust gas can become as high as 500 °C and these temperatures are considerably higher than the temperature of the vehicle body. The exhaust system of a vehicle is the region in which the highest density of infrared radiation energy can be observed [1-3]. The high temperature exhaust gas of special vehicles mainly includes CO_2, H_2O, CO, SO_2, NO_2, NO, HC, and C particles [4, 5], which enter the atmosphere to form a high temperature exhaust jet. When a fluid-flows into another fluid, there is momentum exchange between the inflowing jet fluid and the original fluid. This effect causes a part of the original fluid to move with the jet fluid. This phenomenon is called entrainment effect. With the increasing distance from the nozzle, the high temperature jet continuously mixes

* Corresponding author, e-mail: fengyunsong17@nudt.edu.cn

with the ambient air because of its entrainment effect on the atmosphere. The outer boundary of this jet continuously expands to form a high temperature tail flow field. The high temperature exhaust gas discharged from the exhaust system combines with the dust rolled up by the wheels or tracks to form large pieces of hot soot exhibiting obvious infrared characteristics [6, 7]. With the rapid development of the infrared detection and imaging technology, high temperature exhaust gas, and dust can enable the easy discovery and tracking of special vehicles via infrared imaging systems, considerably threating the safety of such vehicles during wars.

Hence, the infrared radiation associated with the exhaust system of such vehicles must be reduced. Therefore, this study proposes the ejector of cold ambient air to cool the exhaust gas, reducing the infrared radiation intensity associated with the exhaust gas.

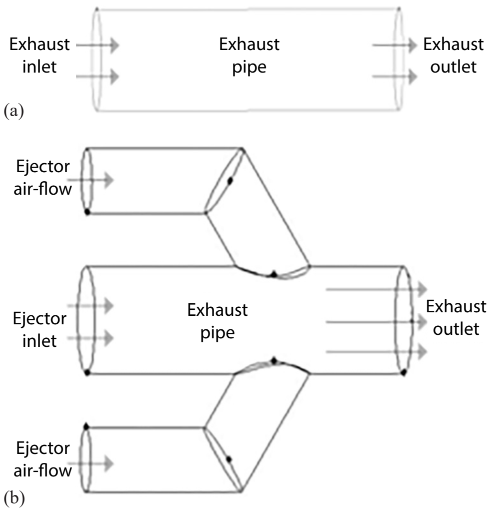

Figure 1. Exhaust pipe models; (a) original exhaust pipe model and (b) proposed exhaust pipe model with ejector

Calculation of the exhaust flow field

In the proposed system, the working fluid is the exhaust gas discharged from the power unit, and the ejector fluid-flowing from the ejector tubes on both the sides is ambient cold air. The working fluid and ejector fluid are discharged after being mixed in the main exhaust pipe, and the velocity and temperature fields gradually become balanced during flow [8, 9]. Thus, the infrared radiation intensity can be reduced by considerably decreasing the temperature of the working fluid. This is the basic principle associated with the ejector of cold air to reduce the temperature of the exhaust gas and exhaust pipe.

The Shaanxi Automobile 2190 chassis manufactured by Shaanxi Automobile Group Co., Ltd. is widely used in special vehicles. Its engine model is WD615.50, the engine displacement is 9726 mL, and the engine power is 206 kW. Its exhaust system structure is similar to those of other special vehicles. Hence, the Shanxi Automobile 2190 exhaust system was selected as the research object in this study. In this system, the tail of the exhaust pipe is a 30 cm long cylinder with a cross-sectional diameter of 10 cm. Accordingly, an exhaust pipe model without the ejector technology was established, as shown in fig. 1(a). Further, a physical model of the ejector exhaust pipe was established for this system based on the principle of injecting cold air, as shown in fig. 1(b) [10]. In this model, the exhaust nozzle is circular with a cross-sectional diameter of 10 cm, and both the ejector tubes have a diameter of 6 cm. The ejector tubes bend at 120° and then enter the main exhaust pipe at an angle of 60°.

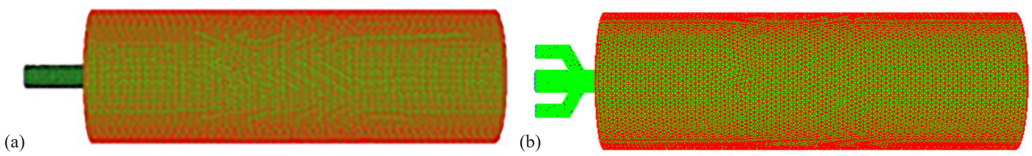

Figure 2. Grid division of the flow-field calculation area; (a) original exhaust pipe model and (b) exhaust pipe model after with ejector

The FLUENT 6.3 software is used to numerically estimate the exhaust flow of a special-vehicle exhaust system to obtain the spatial distribution of various parameters, such as pressure, temperature, and gas component mole fraction, of the special-vehicle exhaust field. First, the shape and size of the flow-field calculation area must be determined using GAMBIT 2.2 software. The shape of the area of the special-vehicle exhaust flow process is numerically estimated to be a cylinder of length l = 180 cm and radius r = 30 cm. The flow-field calculation areas of the original exhaust pipe model and the ejector exhaust pipe model is meshed, and an unstructured tetrahedral grid is used, as shown in fig. 2. Then, the meshed model is imported into FLUENT, and the initial parameters are established. Based on the combustion theory, the mass percentages of N_2, CO_2, O_2, CO, and H_2O at the main inlet are 69.3%, 16.9%, 4.3%, 2%, and 7.5%, respectively. Air is injected from the outside. It comprises N_2 and O_2 with mass percentages of 75.6% and 24.4%, respectively. A speed of 10 m/s and a temperature of 400 K were considered to be the mainstream (engine exhaust) inlet boundary conditions, whereas a speed of 5 m/s and a temperature of 293 K were considered to be the secondary-flow (ejector flow) inlet boundary condition. The nozzle wall was a non-slip frictionless insulating wall. Both the outlet and far-field pressure boundary conditions were a total pressure of 101325 Pa and a temperature of 293 K. Finally, the velocity entry boundary was considered to be the initial face of the calculation, and the velocity value at the boundary was considered to be the initial value when estimating the flow field. In the initialization calculation, both the outlet and far-field pressure boundary conditions do not need to be considered.A non-slip solid boundary condition is adopted for the outlet wall, and the wall surface is set as the coupling surface for the flow and solids. The radiative heat transfer between the wall surfaces is not considered when calculating the temperature field. The external air-flow is maintained constant, and the nozzle wall is insulated without considering the thickness of the nozzle. The flow-field calculation was performed using FLUENT 6.3 software via the couple implicit algorithm. The convergence accuracy was 10^{-4}. The distribution of the static pressure and static temperature of the exhaust gas can be obtained when iterative calculations of the exhaust field performed using the FLUENT software converged, as shown in fig. 3.

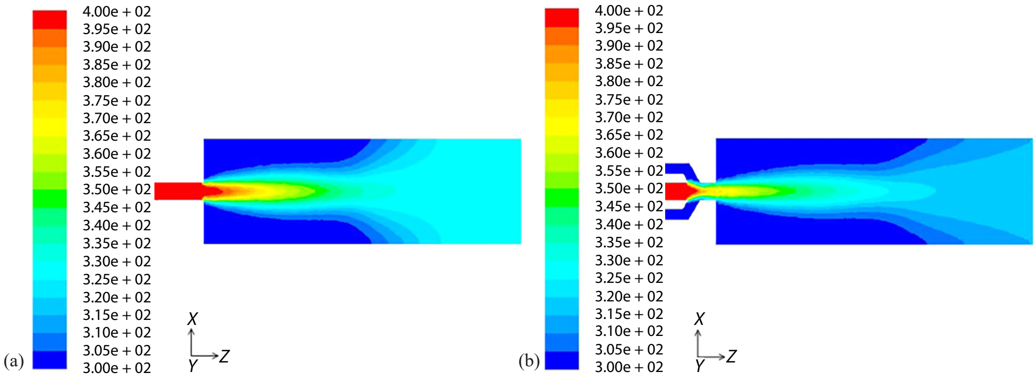

Figure 3. Distribution of the static temperature of exhaust gas at the XOY face when Z = 0 m; (a) original exhaust pipe model and (b) proposed exhaust pipe model

The comparison and analysis of the exhaust-gas field distribution data with respect to the exhaust pipe model before and after the installation of the ejector tube indicated that the pressure of the exhaust gas field was only slightly changed. The pressure was maintained considerably similar to the ambient value of 101325 Pa. In the proposed design, the temperature of the exhaust-gas field decreases rapidly at approximately $Z = 100$ cm. However, in the original design, the exhaust plume temperature was observed to be as high as 330 K when $Z = 180$ cm. The temperature of the exhaust-gas field decreases rapidly in the radial direction, but the density of the exhaust gas is lower than the gas density of the environment. The mole fractions of H_2O, CO, and CO_2 in the exhaust-gas field decrease rapidly in the axial direction, but the N_2 and O_2 contents increase rapidly because of environmental influence.

Gas radiation transfer equation

In case of sufficient combustion, the exhaust gas of the special vehicle engine was assumed to be almost free of solid particles. Therefore, the influence of scattering on infrared radiation can be ignored. Then, the radiative transfer equation [11] can be simplified:

$$\frac{\mathrm{d}L_\lambda\left(s,\vec{r}\right)}{\mathrm{d}s} = -\overline{\alpha}_\lambda\left(s\right)L_\lambda\left(s,\vec{r}\right) + \overline{\alpha}_\lambda\left(s\right)L_{b\lambda}\left(s\right) \tag{1}$$

where λ is the central wavelength of the narrow band, $\vec{r}$ – the position vector, s – the direction vector $\overline{\alpha}_\lambda(s)$ – the mean absorption coefficient of gas, $L_\lambda(s, \vec{r})$ – the spectral radiation in the s-direction of the microbody located at $\vec{r}$, and $L_{b\lambda}(s)$ – the black-body spectral radiation in the s-direction of the microbody.

In case of a statistical narrowband model based on the Lorentzian profile, the average transmittance of the exhaust plume in a certain narrow band is calculated to obtain the mean absorption coefficient. Then, the average transmittance [12, 13] $\overline{t_i}$ can be calculated:

$$\overline{t_l} = \exp\left[-ku\left(1+\frac{kud}{\pi\Delta_C}\right)^{-1/2}\right] \tag{2}$$

where Δ_C, k, d, and u are the half-width, average absorption factor, line spacing, and optical thickness, respectively. After obtaining the average transmittance $\overline{t_i}$, the mean absorption coefficient can be calculated [12]:

$$\overline{\alpha}_l = -\frac{\ln \overline{t_l}(s_a)}{s_a} \tag{3}$$

where s_a is the mean physical length of the microbody.

The plume contains various gases that absorb infrared radiation. The absorption coefficient of each gas was determined and summed to obtain the total absorption coefficient of the plume.

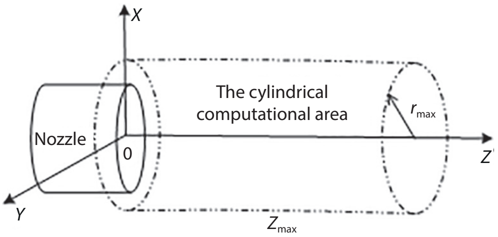

Figure 4. Exhaust cylindrical computational area

Calculation model of the exhaust-gas infrared radiation

Calculation model of infrared radiation brightness

Based on the analysis of the exhaust core area, the exhaust temperature is the highest near the nozzle. However, the exhaust temperature decreases with the increasing radial and axial distances. Accordingly, the influence of the plume on the absorption and emission of infrared radiation decreases. Therefore, the established exhaust temperature Tlimit is considered to be the threshold value with respect to the exhaust-radiation computational area, which can be modified by patching to obtain a cylindrical computational area [14]. The co-ordinate value is considered to be $Z_{\max}$ when the exhaust temperature in the flow field is slightly more than or equal to T_{limit} in the direction of the z-axis. Similarly, $r_{\max}$ in the radial direction can be obtained. Then, $Z_{\max}$ and $r_{\max}$ denote the length and radius of the cylindrical computational area, respectively, as shown in fig. 4. Radiation transmission can be estimated only in the cylindrical computational area, and the exhaust infrared radiation outside this area can be ignored.

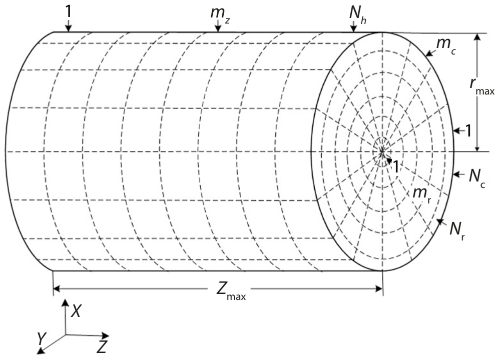

Figure 5. Gridding of the computational area

The cylindrical computational area comprises grids, and $Nr = 10$, $N_c = 16$, and $N_h = 20$, as shown in fig. 5. The serial number of microbody P is (n_r, n_c, n_h), and the volume of the microbody is V_P.

The basic concept associated with the finite volume method is to ensure that the radiant energy of the microcontrol body is conserved with respect to each solid angle. Therefore, the computational region and the 4π space must be spatially discretized and angularly separated [11]. Spatial discretization refers to the discretization of the cylindrical computational area into areas with control volume, V_P, such that the areas do not overlap. Angle dispersion indicates the discretization of the 4π space into solid angles, Ω^m, that do not overlap with each other, as shown in fig. 6. By integrating the radiation transfer, as shown in eq. (1), based on the control volume, V_P, and the control solid angle, Ω^m, and using the Gaussian formula, the finite volume expression of the radiant energy conservation equation can be obtained:

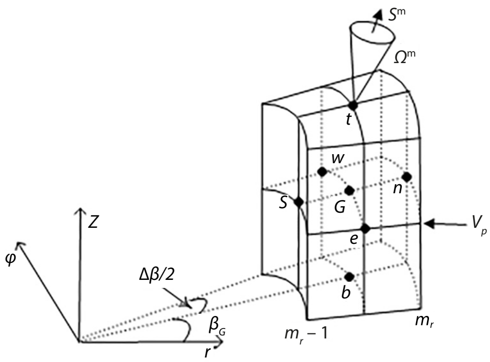

Figure 6. Discrete space and solid angle

$$\int_{\Omega^m}\int_{A_c} L_{l,c}^m (s^m n_j) \mathrm{d}A_c \mathrm{d}\Omega^m = \int_{\Omega^m}\int_{V_P} [-\bar{\alpha}_l (s^m) L_l^m (s^m) + \bar{\alpha}_l (s^m) L_{lb} (s^m)] \mathrm{d}V \mathrm{d}\Omega^m \tag{4}$$

The radiation brightness set in the control solid angle, Ω^m, and the control volume, V_P, is equal, which is approximately represented by the value on the node P in the control volume. The integral term on the right side of eq. (4) can be approximated using a numerical integral:

$$\int_{\Omega^m}\int_{V_P} [-\bar{\alpha}_l (s^m) L_{l,c}^m (s^m) + \bar{\alpha}_l (s^m) L_{lb} (s^m)] \mathrm{d}V \mathrm{d}\Omega^m \approx [-\bar{\alpha}_{l,P} L_{l,P}^m + \bar{\alpha}_{l,P} L_{lb,P}]\Omega^l] V_P \Omega^m \tag{5}$$

For each solid angle, the radiations on the relevant surfaces of the control body are assumed to be equal and are approximately represented as $L_{\lambda,c,j}$ at the integration point j at the center of each outer surface of the control body. If the control body includes M areas and $Q_{l,j}^m$ is the radiant energy obtained by the separation of the j plane with the solid angle Ω^m, then $Q_{l,j}^m$ can be approximated:

$$Q_{l,j}^m = A_{c,j} \int_{\Omega^m} L_{l,c,j}^m (s^m n_j) \mathrm{d}\Omega^m \approx A_{c,j} L_{l,c,j}^m \int_{\Omega^m} (s^m n_j) \mathrm{d}\Omega^m = A_{c,j} L_{l,c,j}^m D_j^m \tag{6}$$

where

$$D_j^m = \int_{\Omega^m} (s^m n_j) \mathrm{d}\Omega.$$

Equation (6) is used to sum the M faces (j = 1, 2, ..., M) of the ring surface of the control body, the sum is substituted into eqs. (4) and (5) to obtain:

$$\sum_{j=1}^{M} A_{c,j} L_{\lambda,c,j}^m D_j^m = [-\bar{\alpha}_{l,P} L_{\lambda,P}^m + \bar{\alpha}_{l,P} L_{\lambda b,P}] V_P \Omega^m \tag{7}$$

The radiation of the control surface of the external body is correlated with that of the center of the control body by selecting the step-difference format. The subscripts J = E, W, S, N, T, and B are used to represent the central node of the control bodies adjacent to the control body P. Equation (7) can be re-written:

$$b_{l,P}^m L_{l,P}^m = \sum_{J=\mathrm{E,W,S,N,T,B}} b_J^m L_{l,J}^m + c_{l,P}^m \tag{8}$$

For the detailed solution method involving $b_{l,P}^m$, b_J^m, and $c_{l,P}^m$, please refer to Ge *et al.* [15]. Equation (8) can be solved via the biconjugate gradient stabilized method [7]. The radiation intensity can be determined after estimating the infrared radiation brightness of the exhaust using the finite volume method.

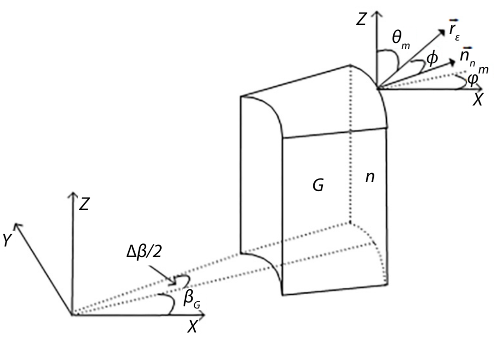

Figure 7. Relative position of the outermost surface normal of the area and the center of the solid angle

Calculation model of infrared radiation intensity

The finite volume method is used to numerically estimate the radiative transfer of the exhaust gas to obtain the directional spectral radiation brightness of the exhaust gas. The radiation-intensity calculation formula must be used to understand the radiation-intensity characteristics of the exhaust gas, and the exhaust-gas radiation intensity can be obtained by further solving this formula.

An arbitrary microcontrol body G located at the outermost side of the cylindrical exhaust-gas calculation area is selected, as shown in fig. 7. According to the dispersion of the cylindrical exhaust-gas computation area, the area A_n of the outer surface n in the control body G can be calculated [16]:

$$A_n = r_{\max} \Delta\beta \Delta h \tag{9}$$

The angle between the unit vector $\vec{r}_\mathrm{e}$ at the center of the control body solid angle Ω^m and the positive direction of the x-axis is θ^m, whereas that between the projection of $\vec{r}_\mathrm{e}$ on the YOZ plane and the positive direction of the z-axis is φ^m. Further, the angle between the normal vector $\vec{n}_n$ of the outer surface of the control body G and $\vec{r}_\mathrm{e}$:

$$\cos\phi = \sin\theta^m \cos(\varphi^m - \beta_G) \tag{10}$$

The spectral radiation intensity can be calculated:

$$\Delta I_l(\theta,\varphi) = L_l(\theta,\varphi)\cos\phi \Delta A \tag{11}$$

By substituting eqs. (9) and (10) into eq. (11), we obtain the following [10]:

$$\Delta I_l(\theta^m,\varphi^m)=L_{l,Gn}(\theta^m,\varphi^m)\sin\theta^m\cos(\varphi^m-\beta_G)r_{\max}\Delta\beta\Delta h \tag{12}$$

where $L_{l,Gn}(\theta^m, \varphi^m)$ is the directional spectral radiation brightness of the outer surface n of the microcontrol body G. Based on the definition of the spatial step-difference format, the radiation brightness of the outer surface n is equal to that of the center of the control body G, *i.e.*, $L_{l,Gn}(\theta^m, \phi^m)$.

At a discrete height h_{m_z} in the cylindrical exhaust area, N_c microcontrollers are present on the outermost side, as shown in fig. 8. The radiation intensity of the outer surface is obtained. The circumferential discrete coding of the microcontrol body G in the exhaust area is m_c. Then, the radiation intensity of the outer surface of the discrete cylindrical exhaust-system outer surface can be obtained [14]:

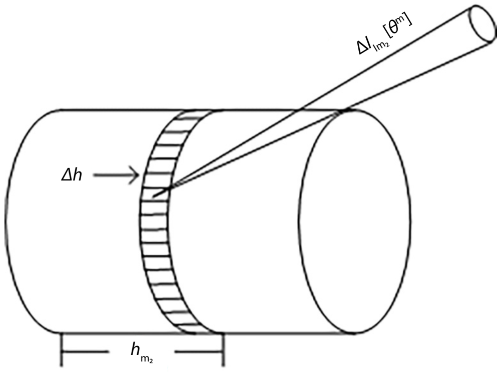

Figure 8. Schematic of the radiation intensity of a cylindrical exhaust system

$$\Delta I_{l,m_z}(\theta^m,\varphi^m)=\sum_{\substack{\beta_G=0\\ \left|\varphi^m-\frac{2\pi m_c}{N_c}\right|<\frac{\pi}{2}}}^{2\pi} L_{l,m_z,m_c}(\theta^m,\varphi^m)\sin\theta^m\cos\left(\varphi^m-\frac{2\pi m_c}{N_c}\right)r_{\max}\Delta\beta\Delta h \tag{13}$$

At a discrete height h_{m_z}, when θ is constant, the radiation brightness of the outermost surface of the cylindrical exhaust:

$$L_{l,m_z,m_c}(\theta,\varphi)=L_{l,m_z,m_c-1}\left(\theta,\varphi-\frac{2\pi}{N_c}\right) \tag{14}$$

where $L_{l,m_z,m_c}(\theta, \varphi)$ is the radiation brightness of the outermost circumferential surface discretely coded as (m_z, m_c). Equation (13) can be simplified as follows if the radiation intensity of the exhaust gas on a certain cylindrical surface is independent of the circumferential angle φ:

$$\Delta I_{l,m_z}(\theta^m)=\sum_{\substack{m_c=1\\ \left|\varphi^m-\frac{2\pi m_c}{N_c}\right|<\frac{\pi}{2}}}^{2\pi} L_{l,m_z,m_c}(\theta^m,\varphi^m)\sin\theta^m\cos\left(\varphi^m-\frac{2\pi m_c}{N_c}\right)r_{\max}\Delta\beta\Delta h \tag{15}$$

Using eq. (15), for the radiation intensity in a certain band $\lambda_1\sim\lambda_2$, the calculation expression can be obtained:

$$\Delta I_{B,m_z}(\theta^m)=\sum_{1}^{N_1}\sum_{\substack{m_c=1\\ \left|\varphi^m-\frac{2\pi m_c}{N_c}\right|<\frac{\pi}{2}}}^{2\pi} L_{l,m_z,m_c}(\theta^m,\varphi^m)\sin\theta^m\cos\left(\varphi^m-\frac{2\pi m_c}{N_c}\right)r_{\max}\Delta\beta\Delta h\Delta\eta \tag{16}$$

where $\Delta\eta$ is the spectral interval of the absorption coefficient calculated using the narrowband model.

Calculation results and analysis

Spectral characteristics of infrared radiation

A control body coded as (9,4,11) on the surface of the calculation area is considered to understand the spectral radiation characteristics of the exhaust gas. The spectral radiation curves of the center of the outer surface along the directions of $\theta = \pi/28$ and $\varphi = \pi/24$, and $\theta = 13\pi/28$ and $\varphi = 11\pi/24$ are shown in fig. 9. This figure shows several clear radiation peaks on the spectral radiation curve of the exhaust gas. The peak radiation wavelengths can be observed at approximately 2.7, 4.3, 5.97, and 6.55. The spectrum is mainly the molecular spectrum of the polyatomic molecular radiation of H_2O and CO_2 because the main component of the exhaust gas is a gas stream comprising H_2O, CO_2, and CO. In the infrared band, the exhaust radiation is mainly generated because of the vibration of heteronuclear polyatomic molecules with inherent dipole moments. The vibration forms are more complex in case of polyatomic molecules such as H_2O, CO_2, and CO. Hence, their radiation shows distinct selective discontinuous spectra. The CO_2 produces two strong absorption bands near 2.7 and 4.3 μm, whereas H_2O produces three strong absorption bands near 2.7, 5.97, and 6.55 μm. The radiation peak at 2.7 μm can be attributed to the combined action of H_2O and CO_2. The radiation of the remaining gas components is relatively weak and does not significantly affect the infrared-radiation spectral characteristics of the exhaust gas. Figure 9 shows that the spectral radiation brightness of the control body changes as the calculation direction changes. As the radiation direction changes, the temperature and optical path length of the radiation transmitted through the exhaust-gas area change, changing the spectral radiation brightness [17].

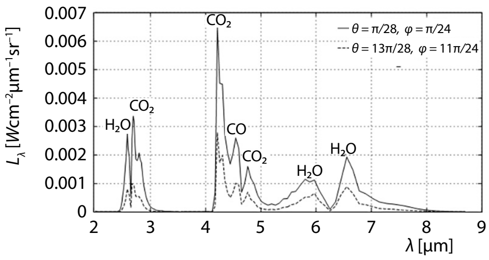

Figure 9. Spectral radiant brightness of the microbody (9,4,11) in different directions

Infrared radiation intensity distribution

After estimating the radiation of the tail flame spectrum, the spatial distributions of the radiation intensity of the special vehicle exhaust gas in the 3-5 μm band in the original pipe model and the proposed model were calculated, and the results are shown in fig. 10. To clearly compare and analyze the spatial distribution characteristics of the mid-infrared radiation intensity of the special-vehicle exhaust before and after the application of the ejector technique, the detection range in the XOZ plane of the symmetry plane is set between −π/2 and π/2 and the detection interval is π/12. The infrared radiation intensity distributions in the exhaust of special vehicles with and without the application of the ejector technique are calculated, as shown

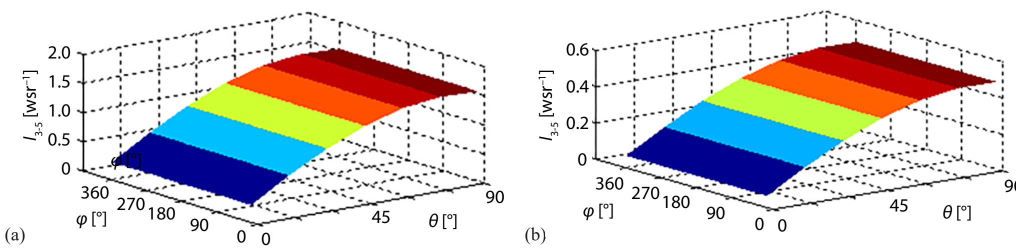

Figure 10. Spatial distribution of the radiation intensity of exhaust gas in the range of 3-5 μm; (a) original design and (b) proposed design

in fig. 11. This figure shows that the infrared radiation intensities of the exhaust gas in the axial direction (θ = 0) are 0.3035 and 0.0661 W/sr with and without the application of the ejector technology, respectively. Thus, in this direction, the exhaust-gas radiation is observed to decrease by 78.2% when using the ejector technique. As θ increases, the infrared radiation intensity of the exhaust gas increases rapidly. In the vertical direction of the exhaust flow (θ = π/2), the infrared radiation intensities of the exhaust gas are 1.546 and 0.481 W/sr before and after the application of ejector technique, respectively. Thus, in this direction, the exhaust-gas radiation is observed to decrease by 68.9% when using the ejector technique.

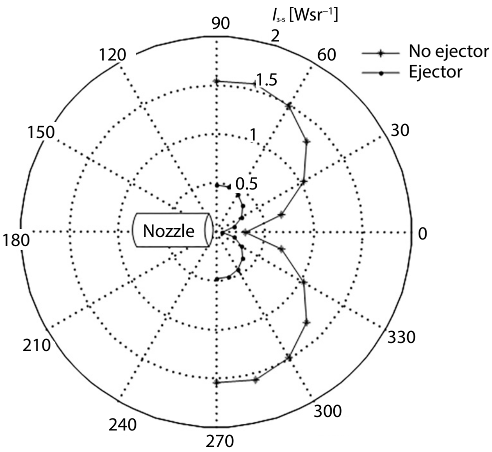

Figure 11. Exhaust-gas-intensity distribution in the 3-5 μm band before and after the application of the ejector technique in the *XOZ* plane

Data analysis showed that the infrared radiation intensity distribution of the vehicle exhaust is axisymmetric and that the infrared radiation is the weakest in the axial direction. The infrared radiation intensity of the exhaust gas considerably decreases by approximately 70% when the ejector technique is applied with respect to the tail nozzle of the vehicle. This is mainly because the ejector technology introduces cold air, considerably reducing the temperature of the exhaust gas. Therefore, the use of ejector technology in the tailpipe of special vehicles will effectively suppress their infrared radiation.

Experimental verification

The ejector model was designed and processed based on the results of theoretical calculations to verify the credibility of the numerical calculations. The Shaanxi Automobile 2190 exhaust system was the research object, and a dynamic test was conducted to suppress the exhaust-gas infrared radiation by injecting air. The FLIR T630 thermal imaging camera was used to evaluate the infrared characteristics of the exhaust pipe before and after injecting the cold air, as shown in fig. 12. The infrared radiation of the exhaust pipe was observed to decrease considerably with the ejector of cold air. Thus, the reliability of the theoretical calculation and the rationality of the ejector model design were validated.

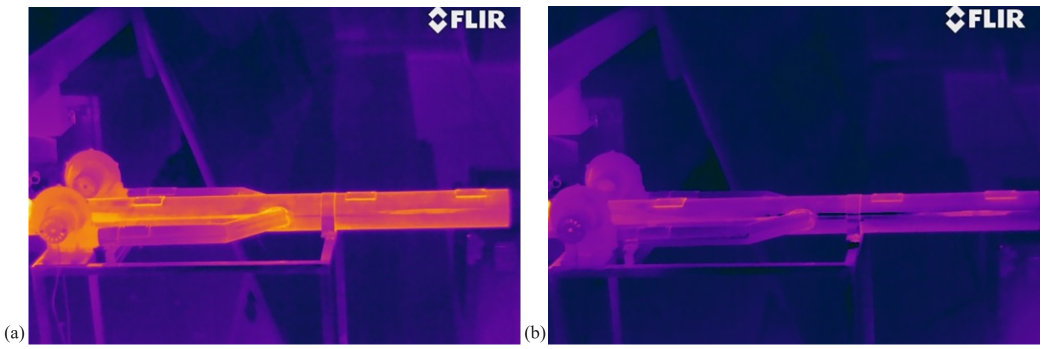

Figure 12. Infrared thermal images of the exhaust pipe before and after the ejector of cold air; (a) before the ejector of cold air and (b) after the ejector of cold air

Conclusion

In this study, the exhaust flow field outside the exhaust pipe of a special vehicle was numerically calculated before and after using the ejector technology. Based on this calculation, the finite volume method and the narrowband model of gas radiation were used to estimate the infrared radiation characteristics of the vehicle exhaust and its medium-wave infrared radiation intensity distribution. The following conclusions were obtained by analyzing the calculation results.

- Two radiation peaks are observed at 2.7 and 4.3 μm within the atmospheric window of 3-5 μm, the brightness is greater at the latter peak.
- The infrared radiation intensity distribution of the special-vehicle exhaust gas is axisymmetric, and its infrared radiation is the weakest in the axial direction.
- The application of the ejector technology in the tail nozzle of a special vehicle considerably reduced the infrared radiation intensity of the exhaust gas by approximately 70%. Therefore, the usage of this technology in the tail nozzle of special vehicles will effectively suppress the infrared radiation associated with such vehicles.

Acknowledgment

This work is supported by the National Nature Science Foundation of China (61405248).

Nomenclature

$\Delta I_l(\theta^m, \varphi^m)$ – radiation intensity of the discrete cylindrical exhaust outer surface [$\mathrm{Wsr^{-1}}$]

$L_\lambda(s, \vec{r})$ – spectral radiation brightness in the s-direction of the microbody located at $\vec{r}$, [$\mathrm{Wcm^{-2}\mu m^{-1}sr^{-1}}$]

$\overline{t_l}$ – average transmittance, [–]

Greek symbols

$\overline{\alpha}_\lambda(s)$ – mean absorption coefficient of the gas, [–]

λ – central wavelength of a narrow band, [μm]

Ω^m – solid angle, [sr]

References

[1] Jellison, G. P., *et al*., Determination of Gas Plume Temperature from Molecular Emission Spectra, *Optical Engineering*, *45* (2006), 1, 016201-1-8

[2] Kokkulunk, G., *et al*., Prediction of Emissions and Exhaust Temperature for Direct Injection Diesel Engine with Emulsified Fuel Using ANN, *Turkish Journal of Electrical Engineering and Computer Sciences*, *21* (2013), 2, pp. 2141-2152

[3] Khan, M. M., *et al*., Exhaust Plume Flow Visualization for Qualitative Analysis of Engine Combustion Rerformance, *IEEE Transactions on Plasma Science*, *37* (2009), 6, pp. 1-6

[4] Muda, R., *et al*., Simulation and Measurement of Carbon Dioxide Exhaust Emissions Using an Optical-Fibre-Based Mid-Infrared Point Sensor, *Journal of Optics A-Pure and Applied Optics*, *11* (2009), 5, pp. 234-341

[5] Yoo, D. H., *et al*., Masaru IKAME Exhaust IR Characteristics of Nitrous Oxide from Marine Engine, *IEEE Oceans*, *42* (2012), 4, pp. 121-129

[6] Blunck, D., *et al*., Radiating Characteristics of High Temperature Exhaust Plumes from a Subsonic Axisymmetric Nozzle, *Proceedings*, 47th AIAA Aerospace Sciences Meeting including the New Horizons Forum and Aerospace Exposition, Orlando, Fla., USA, 2009, AIAA-2009-1639

[7] Faria, R. I., *et al*., A Prediction of Distribution Transformers Aging Based on Tank Infrared Temperature Measurements, *Proceedings*, 22nd International Conference and Exhibition on Electricity Distribution, Stockholm, Sweden, 2013, Vol. 2013-1212

[8] Sun, X., *et al*., Thermal Analysis and Cooling System Design of Dual Mechanical Port Machine for Wind Power Application, *IEEE Transactions on Industrial Electronics*, *60* (2013), 5, pp. 1724-1733

[9] Waung, T., *et al*., An Ejector Air Intake Design Method for a Novel RBCC Rocket Nozzle, *Proceedings*, 45th AIAA/ASME/SAE/ASEE Joint Propulsion Conference & Exhibit, Denver, Col., USA, 2009, AIAA-2009-5294

[10] Li, J., *et al*., Study on Infrared Suppressor Ejected by Armored Vehicle Exhaust, *Journal of Sichuan Ordnance*, *32* (2011), 10, pp. 70-73
[11] Tan, H. P., *et al*., Numerical Claculation of Transmission and Characteristic of Infrared Radiation, *Publishing House of Haerbin Industrial University*, Harbin, China, 2006
[12] Liu, F. S., *et al*., The 3-D Non-Grey Gas Radiative Transfer Analyses Using the Statistical Narrow-Band Model, *International Journal of Heat Mass Transfer*, *37* (1998), 9, pp. 759-768
[13] Ludwing, C. B., *et al*., Hand-Book of Infrared Radiation from Combustion, Report NASA-SP-3080, USA, 1973
[14] Feng, Y., *et al*., Numerical Calculation on Infrared Characteristics of the Exhaust Plume Outside Axial-Symmetrical Nozzle, *Proceedings*, International Symposium on Infrared Technology and Application and the International Symposiums on Robot Sensing and Advanced Control, Beijing, China, 2016, Vol. 10157-101571G
[15] Ge, L., *et al*., Simulation of Infrared Radiation of IRSS System, *Infrared and Laser Engineering*, *39* (2010), 6, pp. 1003-1006
[16] Jin, W., *et al*., Numerical Simulation of Infrared Radiation of Satellite Attitude Thruster Plume, *Infrared and Laser Engineering*, *40* (2011), 4, pp. 595-599
[17] Feng, Y., *et al*., Numerical Calculation on Infrared Characteristics of the Special Vehicle Exhaust System, *Proceedings*, Applied Optics and Photonics China: Optical Spectroscopy and Imaging, Beijing, China, 2017, Vol. 10461-104611L

Paper submitted: June 11, 2020
Paper revised: August 30, 2020
Paper accepted: September 23, 2020